2019 IEEE 58th Conference on Decision and Control (CDC)
Palais des Congrès et des Expositions Nice Acropolis
Nice, France, December 11-13, 2019

Drag reduction in turbulent channel flow over spatially periodic surfaces

Wei Ran, Armin Zare, and Mihailo R. Jovanović

***Abstract*— Carefully designed surface corrugation is a sensor-free strategy that can reduce skin-friction drag in turbulent flows. In contrast to the traditional approach that relies on numerical simulations and experiments, we develop a model-based framework to quantify the impact of spanwise-periodic surfaces on the dynamics of velocity fluctuations and the resulting mean flow. We model the effect of surface corrugation as a volume penalization on the Navier-Stokes equations and use the statistical response of the stochastically forced linearized equations to quantify the effect of background turbulence on skin-friction drag. For triangular corrugations, we demonstrate that our simulation-free approach reliably predicts drag-reducing trends observed in high-fidelity simulations and experiments.**

***Index Terms*— Drag reduction, sensor-free flow control, spatially-periodic systems, spatio-temporal frequency responses, stochastically-forced Navier-Stokes, turbulence modeling.**

I. Introduction

A. Background

Carefully designed surface corrugation can decrease skin-friction drag by more than 10% [1], [2] and has been successfully employed in engineering applications [3], [4]. Previous numerical and experimental studies have examined the effect of various design parameters, e.g., the shape (triangular, T-shaped, etc.) and size of riblets, on skin-friction drag in turbulent flows [1], [5]–[8]. Moreover, the drag-reducing nature of corrugated surfaces has been linked to the creation of secondary streamwise vortices at riblet tips [9] or susceptibility to a Kelvin-Helmholtz instability [10]. While these studies offer valuable insights, their reliance on costly experiments and simulations has hindered the model-based design of riblet-mounted surfaces. This motivates the development of low-complexity models that capture the essential physics of turbulent flows over riblets and are well-suited for analysis, optimization, and control design.

The linearized Navier-Stokes (NS) equations capture structural and statistical features of transitional [11]–[14] and turbulent [15]–[17] shear flows. An additive source of stochastic excitation is often used to model the effect of background disturbances and uncertainty in the linearized equations. This approach has enabled the model-based analysis of sensor-free strategies for suppressing turbulence via streamwise traveling surface blowing and suction [18], [19] or transverse wall oscillations [20], [21]. In this paper, we extend the framework of [21] to account for the effect of spanwise-periodic surface modification using tools from control theory. We use turbulence modeling in conjunction with stochastically-forced linearized NS equations to compute modifications to the turbulent mean velocity and skin-friction drag in a channel flow with corrugated walls. This is an unconventional sensor-free boundary control problem; the goal is to quantify the influence of the fluctuation velocity field induced by spatially-periodic boundary conditions on the mean velocity profile and the resulting skin-friction drag.

Receptivity of channel flow over riblets was recently studied using the $\mathcal{H}_2$ norm of the linearized dynamics [22], as well as frequency response analysis [23]. In [22], a change of coordinates was used to translate spatially-periodic boundary conditions into spatially-periodic differential operators and, in [23], a volume penalization technique [24] was used to capture the effect of riblets as a feedback term in the dynamics. While we adopt the latter approach, in contrast to prior studies, we account for dynamical interactions among fluctuation harmonics in the spatially-periodic model and utilize the linearized NS equations to provide closure in the mean flow equations for flows over riblets. Our results capture the drag-reducing properties of triangular riblets which are in excellent agreement with simulations and experiments [1], [10]. We also study the kinetic energy of velocity fluctuations and observe a synchrony between energy suppression trends and drag-reduction trends for riblets of various size.

B. Problem formulation

Consider a three-dimensional pressure-driven turbulent channel flow of incompressible Newtonian fluid. In Fig. 1(a), x, $y \in [-1,\, 1]$, and z denote the streamwise, wall-normal, and spanwise coordinates, respectively. The fully-developed turbulent flow is governed by the NS equations

$$\begin{aligned} \mathbf{u}_t &= -(\mathbf{u}\cdot\nabla)\,\mathbf{u} - \nabla P + \frac{1}{Re_\tau}\Delta\mathbf{u} \\ 0 &= \nabla\cdot\mathbf{u} \end{aligned} \tag{1}$$

where $\mathbf{u}$ is the velocity vector, P is the pressure, ∇ is the gradient operator, and $\Delta = \nabla\cdot\nabla$ is the Laplacian, and t is time. The friction Reynolds number $Re_\tau = u_\tau h/\nu$ is defined in terms of the channel's half-height h and the friction velocity $u_\tau = \sqrt{\tau_w/\rho}$, where τ_w is the wall-shear stress (averaged over horizontal directions and time), ρ is the fluid density, and ν is the kinematic viscosity. All variables

Financial support from the Office of Naval Research under Award N00014-17-1-2308 and the Air Force Office of Scientific Research under Awards FA9550-16-1-0009 and FA9550-18-1-0422 is gratefully acknowledged.

Wei Ran is with the Department of Aerospace and Mechanical Engineering, University of Southern California, Los Angeles, CA 90089. Armin Zare is with Department of Mechanical Engineering, University of Texas at Dallas, Richardson, Texas 75080, USA. Mihailo R. Jovanović is with the Ming Hsieh Department of Electrical and Computer Engineering, University of Southern California, Los Angeles, CA 90089. E-mails: wran@usc.edu, armin.zare@utdallas.edu, mihailo@usc.edu.

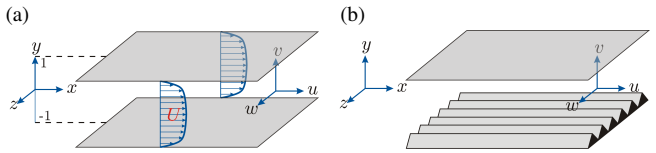

Fig. 1. (a) Fully-developed turbulent channel flow. (b) A channel with spanwise-periodic riblets on the lower wall.

in Eqs. (1) have been non-dimensionalized: length by h, velocity by u_τ, time by h/u_τ, and pressure by ρu_τ^2.

When the lower wall is a spanwise-periodic surface aligned with the flow as shown in Fig. 1(b), the no-slip and no penetration boundary conditions are given by,

$$\mathbf{u}(x, y = 1, z, t) \;=\; 0, \quad \mathbf{u}(x, y = -1 + r(z), z, t) \;=\; 0 \quad (2)$$

where $r(z)$ represents the shape of the surface corrugation. Solving the NS equations (1) subject to these boundary conditions is computationally expensive. This motivates the development of low-complexity models for analysis and optimization purposes. The key challenge is capturing the effect of riblets on the multi-scale nature of the turbulent flow so that skin-friction drag is accurately predicted.

C. Paper outline

In Section II, we present the governing equations for the turbulent mean velocity along with the turbulent viscosity model. We also describe a procedure for determining an approximation to the turbulent mean velocity and skin-friction drag in the flow over riblets. In Section III, we use the linearized NS equations to obtain second-order statistics of velocity fluctuations in channel flow over riblets and compute modifications to the mean velocity and skin-friction drag. In Section IV, we demonstrate the utility of our framework in capturing drag-reducing trends in turbulent flow over riblets. Finally, we provide concluding remarks in Section V.

II. Turbulent mean velocity

As skin-friction drag depends on the gradient of the turbulent mean velocity at the wall, the first step in our analysis is to determine an approximation to the mean velocity in the presence of riblets. For this purpose, we adopt the Reynolds decomposition to split the velocity field into its time-averaged mean and fluctuating parts as

$$\begin{aligned} \mathbf{u} \;&=\; \bar{\mathbf{u}} \,+\, \mathbf{v}, \qquad \mathbf{E}(\mathbf{u}) \;=\; \bar{\mathbf{u}}, \qquad \mathbf{E}(\mathbf{v}) \;=\; 0 \\ P \;&=\; \bar{P} \,+\, p, \qquad \mathbf{E}(P) \;=\; \bar{P}, \qquad \mathbf{E}(p) \;=\; 0. \end{aligned} \quad (3)$$

Here, $\mathbf{E}(\cdot)$ denotes the expectation operator, $\bar{\mathbf{u}} = [U \;\; V \;\; W]^T$ is the vector of mean velocity components, $\mathbf{v} = [u \;\; v \;\; w]^T$ is the vector of velocity fluctuations, and p is the fluctuating pressure field around the mean $\bar{P}$. Substituting (3) into Eqs. (1) and taking the expectation yields the Reynolds-averaged NS equations

$$\begin{aligned} \bar{\mathbf{u}}_t \;&=\; -\,(\bar{\mathbf{u}}\cdot\nabla)\,\bar{\mathbf{u}} \,-\, \nabla\bar{P} \,+\, \frac{1}{Re_\tau}\Delta\bar{\mathbf{u}} \,-\, \nabla\cdot\mathbf{E}(\mathbf{v}\mathbf{v}^T) \\ 0 \;&=\; \nabla\cdot\bar{\mathbf{u}}. \end{aligned} \quad (4)$$

The Reynolds stress tensor $\mathbf{E}(\mathbf{v}\mathbf{v}^T)$ quantifies the transport of momentum arising from turbulent fluctuations [25], and its value affects the solution of Eqs. (4). The fluctuation correlations are, however, difficult to obtain because the nth velocity moment depends on the $(n+1)$th moment (closure problem). To overcome this, we utilize the turbulent viscosity hypothesis [25], which considers the turbulent momentum to be transported in the direction of mean rate of strain

$$\mathbf{E}\left(\overline{\mathbf{v}\mathbf{v}^T}\right) - \frac{1}{3}\mathrm{tr}\left(\mathbf{E}\left(\overline{\mathbf{v}\mathbf{v}^T}\right)\right)I \;=\; -\frac{\nu_T}{Re_\tau}\left(\nabla\bar{\mathbf{u}} + (\nabla\bar{\mathbf{u}})^T\right).$$

Here, $\nu_T(y)$ is the turbulent eddy viscosity normalized by kinetic energy, overline denotes averaging over horizontal dimensions, $\mathrm{tr}(\cdot)$ is the trace, and I is the identity operator.

A. Modeling surface corrugation

To account for the effect of riblets we use the volume penalization technique proposed by Khadra et al. [24]. This method avoids the implementation of boundary conditions in complex geometries by modeling the effect of solid obstructions of the flow as a spatially varying permeability function $K(x,\, y,\, z)$ that influences the governing equations as an additive body force. Based on this modulation, the mean flow equations in steady state take the following form:

$$\begin{aligned} 0 \;&=\; -\,(\bar{\mathbf{u}}\cdot\nabla)\,\bar{\mathbf{u}} \,-\, \nabla\bar{P} \,-\, K^{-1}\,\bar{\mathbf{u}} \\ &\quad + \frac{1}{Re_\tau}\nabla\cdot\left((1 \,+\, \nu_T)(\nabla\bar{\mathbf{u}} \,+\, (\nabla\bar{\mathbf{u}})^T)\right) \\ 0 \;&=\; \nabla\cdot\bar{\mathbf{u}}. \end{aligned} \quad (5)$$

Within the fluid, the penalization resulting from the permeability function K should have no influence on the flow, i.e., $K \to \infty$, yielding back the original mean flow Eqs. (4). On the other hand, within the riblets, the function K should force the velocity field to zero, i.e., $K \to 0$. To respect the shape of the streamwise-constant surface corrugation studied in this paper, we follow [23], [26] and consider the expansion

$$K^{-1}(y, z) \;=\; \sum_{m\in\mathbb{Z}} a_m(y)\exp(\mathrm{i}\, m\,\omega_z z). \quad (6)$$

Here, ω_z is the fundamental spatial frequency of the riblets and $a_m(y)$ specifies their height. The coefficients $a_m(y)$ in (6) can be obtained from the spatial Fourier transform of a pre-determined resistance field $K^{-1}(y, z)$ in the homogeneous direction (z). Figure 2(a) shows the resistance field K^{-1} for triangular riblets with $\omega_z = 30$.

The base flow which is obtained from solving the mean flow Eqs. (5) adopts a similar harmonic form as (6), i.e.,

$$\bar{\mathbf{u}}(y,\, z) \;=\; \sum_{m\in\mathbb{Z}} \bar{\mathbf{u}}_m(y)\exp(\mathrm{i}\, m\,\omega_z z). \quad (7)$$

Remark 1: The solution to nonlinear Eqs. (5) obtained via Newton's method has a single streamwise component, $\bar{\mathbf{u}} = [U(y, z) \;\; 0 \;\; 0]^T$, which significantly simplifies the form of Eqs. (5) bringing them into a linear form.

B. Turbulent drag reduction with ν_{T0}

In order to determine the influence of surface corrugation on drag we need robust models for turbulent viscosity ν_T in

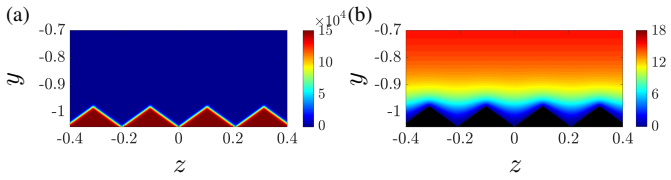

Fig. 2. (a) Resistance field K^{-1} based on Eq. (6) with $m = -12, \ldots, 12$ demonstrating the shape of riblets; and (b) the streamwise mean velocity for turbulent channel flow with $Re_\tau = 186$ over the triangular riblets with $\omega_z = 30$ shown in (a).

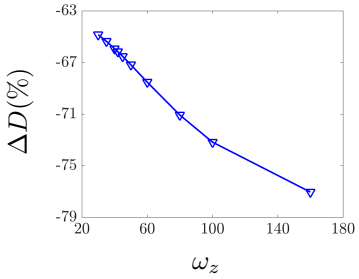

Fig. 3. Drag reduction in a turbulent channel flow with $Re_\tau = 186$ over triangular riblets with various spanwise frequencies ω_z.

Eqs. (5). Several studies have proposed expressions for ν_{T0} that yield the turbulent mean velocity in flows over smooth walls [27]–[29]. Following [21, Section 2.1], we use the Cess turbulent viscosity model $\nu_{T0}(y)$ developed in [29].

In this study, we adjust the wall-normal position of riblets so that the mean velocity profile obtained from (5) has the same bulk, U_B, as the channel flow with smooth walls, i.e.,

$$\frac{\omega_z}{2\pi}\int_{-1}^{1}\int_{0}^{2\pi/\omega_z} U(y,z)\,\mathrm{d}z\,\mathrm{d}y \;=\; \int_{-1}^{1} U_0(y)\,\mathrm{d}y \;=\; U_B.$$

Here, $U_0(y)$ is the turbulent mean velocity profile in the absence of riblets. In the vicinity of the solid wall, the flow is dominated by viscosity and can be assumed to be laminar. Thus, when the size of the riblets are small, the grooved region in between riblets is in close proximity of the solid surface, and can be regarded as a laminar flow regime. Based on this, in this study, we will assume the riblets to be small and consider the flow to be laminar below $y = -1$, i.e., $\nu_T = 0$ for $y \le -1$. A pseudospectral scheme with Chebyshev polynomials [30] is applied to discrete Eqs. (5) in the wall-normal dimension. To avoid numerical oscillations in the solution to Eqs. (5), we divide the wall-normal extent of the computational domain into two parts ($y \le -1$ and $-1 \le y \le 1$) and use block operators [31] to discretize the domains using $N_i = 179$ collocation points for $y \in [-1, 1]$ and $N_o = 20$ collocation points for $y \le -1$.

We impose no-slip boundary conditions (2) on the upper wall of the channel. The adopted volume penalization method automatically enforces immersed boundary conditions on the non-smooth lower wall without the need for additional boundary conditions. The boundary conditions at the intersection of the aforementioned wall-normal regimes ($y = -1$) enforce smoothness of all physical quantities

$$\begin{aligned} \bar{\mathbf{u}}(y = -1^+, z) &= \bar{\mathbf{u}}(y = -1^-, z) \\ \frac{\mathrm{d}\bar{\mathbf{u}}}{\mathrm{d}y}(y = -1^+, z) &= \frac{\mathrm{d}\bar{\mathbf{u}}}{\mathrm{d}y}(y = -1^-, z) \end{aligned} \tag{8}$$

where $y = -1^+$ denotes the lower boundary point at $y = -1$ for the domain over $y \in [-1, 1]$ and $y = -1^-$ is the upper boundary point for the domain over $y \le -1$.

We solve Eqs. (5) with ν_{T0} and pressure gradient $\bar{P}_x = -1$ for $m = -12, \ldots, 12$. Figure 2(b) shows the mean velocity of a turbulent channel flow with $Re_\tau = 186$ over triangular riblets with $\omega_z = 30$. The slope of the mean velocity at the lower wall determines the skin-friction drag

$$D \;=\; \frac{\omega_z}{2\pi}\int_0^{2\pi/\omega_z} \frac{\mathrm{d}U}{\mathrm{d}y}(y = -1, z)\,\mathrm{d}z.$$

The drag reduction rate can thus be computed as

$$\Delta D \;:=\; (D \,-\, D_0)\,/D_0 \tag{9}$$

where D_0 denotes the slope of the mean velocity at the lower wall of a smooth channel (without riblets). Figure 3 shows the percentage of drag reduction obtained using ν_{T0} for a turbulent channel flow with $Re_\tau = 186$. Clearly the amount of drag reduction is significantly over-predicted relative to the rates reported in numerical and experimental studies ($\sim 10\%$). In the next section, we extend the framework proposed in [21] to account for the effect of velocity fluctuations and obtain corrections to the turbulent viscosity ν_{T0}.

III. Dynamics of Velocity Fluctuations

In this section, we examine the dynamics of fluctuations around the turbulent mean velocity profile determined in Section II. The second-order statistics of velocity fluctuations obtained using the stochastically forced linearized equations around $\bar{\mathbf{u}}$ are used to compute corrections to the turbulent viscosity and mean flow profiles. Our model-based framework for studying the effect of surface corrugation involves the following steps:

1) The turbulent mean velocity is obtained from Eqs. (5), where closure is achieved using the turbulent viscosity ν_{T0} for the channel flow with smooth walls.
2) [Section III-D] The stochastically forced linearized NS equations around the mean flow obtained in step 1 are used to compute the second-order statistics of the fluctuating velocity field and correct ν_{T0}.
3) The modified turbulent viscosity is used to correct the mean velocity and compute skin-friction drag.

A. Model equation for ν_T

As mentioned in Section II, ν_{T0} is not an accurate eddy-viscosity model for the channel flow with corrugated surfaces. The challenge stems from connecting ν_T to the second-order statistics of velocity fluctuations. For this purpose, herein, we follow [21] in using the model equation [32]

$$\nu_T(y) \;=\; c\,Re_\tau^2\,\frac{k^2(y)}{\epsilon(y)} \tag{10}$$

where $c = 0.09$, k is turbulent kinetic energy, and ϵ is its rate of dissipation. Wall-normal profiles for k and ϵ can be obtained by averaging the second-order statistics of velocity fluctuations over the horizontal dimensions; see [21, Section 2.3] for details. We next demonstrate how second-order statistics of the fluctuation field can be computed using the stochastically forced linearized NS dynamics.

B. Linearized NS equations

The dynamics of velocity $\mathbf{v} = [\,u\ \ v\ \ w\,]^T$ and pressure p fluctuations around $\bar{\mathbf{u}} = [\,U(y,z)\ \ 0\ \ 0\,]^T$ are governed by the linearized NS and continuity equations:

$$\begin{aligned} \mathbf{v}_t \ &= \ -\,(\nabla\cdot\bar{\mathbf{u}})\,\mathbf{v} \ - \ (\nabla\cdot\mathbf{v})\,\bar{\mathbf{u}} \ - \ \nabla p \ - \ K^{-1}\mathbf{v} \\ &\quad + \ \frac{1}{Re_\tau}\nabla\cdot\big((1+\nu_T)(\nabla\mathbf{u} \ + \ (\nabla\mathbf{u})^T)\big) \ + \ \mathbf{f} \\ 0 \ &= \ \nabla\cdot\mathbf{v}. \end{aligned} \tag{11}$$

Here, $\mathbf{f}$ is a zero-mean white-in-time stochastic forcing. Note that the solution to Eqs. (11) adopts a similar harmonic structure as coefficients K^{-1} and $\bar{\mathbf{u}}$. Following [18], application of the Fourier transform brings the set of spatially periodic PDEs (11) into the evolution form

$$\begin{aligned} \partial_t\boldsymbol{\psi}_\theta(y,k_x,t) \ &= \ A_\theta(k_x)\,\boldsymbol{\psi}_\theta(y,k_x,t) \ + \ \mathbf{f}_\theta(y,k_x,t), \\ \mathbf{v}_\theta(y,k_x,t) \ &= \ C_\theta(k_x)\,\boldsymbol{\psi}_\theta(y,k_x,t) \end{aligned} \tag{12}$$

where the state $\boldsymbol{\psi} = [\,v\ \ \eta\,]^T$ contains wall-normal velocity v and vorticity $\eta = \partial_z u - \partial_x w$. At the upper-wall of the channel, homogenous Dirichlet boundary conditions are imposed on η, while homogeneous Dirichlet and Neumann boundary conditions are imposed on v. Similar to the mean flow equations (5), the boundary conditions at the corrugated surface are automatically satisfied via volume penalization.

In Eqs. (12), $\boldsymbol{\psi}_\theta$, $\mathbf{v}_\theta$, and $\mathbf{f}_\theta$ are bi-infinite column vectors parameterized by the spanwise wavenumber offset $\theta \in [0, \omega_z/2)$ and the streamwise wavenumber k_x. For example, $\boldsymbol{\psi}_\theta(y,k_x,t) = \mathrm{col}\{\boldsymbol{\psi}(\theta_n,y,k_x,t)\}_{n\in\mathbb{Z}}$, where $\theta_n = n\omega_z + \theta$ for various harmonics $n\,\omega_z$. Furthermore, for each θ and k_x, $A_\theta(k_x)$ and $C_\theta(k_x)$ are bi-infinite matrices whose elements are integro-differential operators in y; see Appendix A.

C. Second-order statistics of velocity fluctuations

The linearized dynamics (12) are driven by zero-mean white-in-time stochastic forcing $\mathbf{f}$ with second-order statistics

$$\mathbf{E}\,(\mathbf{f}_\theta(\cdot,k_x,t_1)\otimes\mathbf{f}_\theta(\cdot,k_x,t_2)) = M_\theta(k_x)\,\delta(t_1 - t_2). \tag{13}$$

Here, δ is the Dirac delta function, $\otimes$ denotes the tensor product, and $M_\theta(k_x)$ is the spatial spectral-density of forcing. Following [21, Section 3.1], we select M so that the energy spectrum of velocity fluctuations $\mathbf{v}$ matches that of a turbulent channel flow with smooth walls.

The steady-state autocorrelation operator of $\boldsymbol{\psi}_\theta$ can be determined from the solution to the Lyapunov equation

$$A_\theta(k_x)\,X_\theta(k_x) \ + \ X_\theta(k_x)\,A_\theta^\dagger(k_x) \ = \ -M_\theta(k_x)$$

where $\dagger$ denotes the adjoint of an operator which should be determined with respect to the appropriate inner product [13]. The solution X_θ has a similar bi-infinite structure as A_θ in which the (i,j)th block is the correlation matrix associated with the ith and jth harmonics of the state $\boldsymbol{\psi}_\theta$. Due to linearity of the dynamics, autocorrelation matrices $X_d(k_x,\theta_n)$, which represent the elements on the main diagonal of X_θ can be decomposed as

$$X_d(k_x,\theta_n) \ = \ X_0(k_x,\theta_n) \ + \ X_c(k_x,\theta_n) \tag{14}$$

where X_0 and X_c are autocorrelations of velocity fluctuations in the channel with smooth walls and the modification resulting from inclusion of surface corrugation, respectively. Finally, we note that the energy spectrum is given by

$$E(k_x,\theta) \ = \ \mathrm{tr}\,(X_\theta(k_x)) \ = \ \sum_{n\in\mathbb{Z}}\mathrm{tr}\,(X_d(k_x,\theta_n))\,.$$

D. Correction to turbulent viscosity ν_T

According to Eq. (10), the turbulent viscosity ν_T is determined by second-order statistics of the velocity fluctuations. These statistics can be obtained from the autocorrelation operator X_d in (14). Following Eq. (14), the kinetic energy k and its rate of dissipation ϵ can also be decomposed as

$$k \ = \ k_0 \ + \ k_c, \quad \epsilon \ = \ \epsilon_0 \ + \ \epsilon_c \tag{15}$$

where the subscript 0 denotes quantities in the channel flow without surface corrugation, and the subscript c quantifies the influence of fluctuations in the flow over the corrugated surface. While k_0 and ϵ_0 can be extracted from the result of numerical simulations of turbulent channel flows with smooth walls, corrections k_c and ϵ_c can be determined from second-order statistics in $X_c(k_x,\theta_n)$; see [21, Appendix D] for details. Substituting k and ϵ from (15) into (10) and application of the Neumann series expansion yields

$$\nu_T \ = \ \nu_{T0} \ + \ \nu_{Tc} \tag{16}$$

with

$$\nu_{Tc} \ = \ \nu_{T0}\left(\Big(1 \ + \ \frac{k_c}{k_0}\Big)^2\Big(1 \ - \ \frac{\epsilon_c}{\epsilon_0} \ + \ \big(\frac{\epsilon_c}{\epsilon_0}\big)^2\Big) \ - \ 1\right)$$

as the correction to turbulent viscosity ν_{T0}. The influence of fluctuations on the turbulent mean velocity (and consequently drag) can be obtained by substituting ν_T from (16) and solving Eqs. (5). Additional details on computing U_c are omitted for brevity; see [21, Appendix E] for details.

IV. Results

We study the effect of triangular surface corrugation on the skin-friction drag and kinetic energy of turbulent channel flow with $Re_\tau = 186$. The ratio between the height h and spacing $s = 2\pi/\omega_z$ of riblets is assumed to be fixed ($h/s = 0.36$). Second-order statistics of the flow without riblets are provided by high-fidelity simulations [33], [34] and are used to obtain the turbulent energy spectrum of stochastic forcing $\mathbf{f}$ in Eq. (13) and to compute the kinetic energy profile $k_0(y)$ from which $\epsilon_0(y)$ is obtained as $\epsilon_0 = c\,Re_\tau^2 k_0^2/\nu_{T0}$. We use 199 Chebyshev collocation points to discretize the wall-normal dimension ($N_i = 179$, $N_o = 20$). For the horizontal

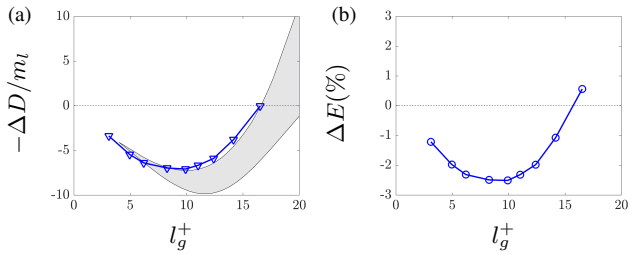

Fig. 4. (a) Normalized turbulent drag reduction (m_l is the slope of the drag reduction curve at small l_g^+) and (b) kinetic energy suppression in a channel flow with $Re_\tau = 186$ over triangular riblets of various size. The shaded area is the envelope of experimental and numerical results [1], [10].

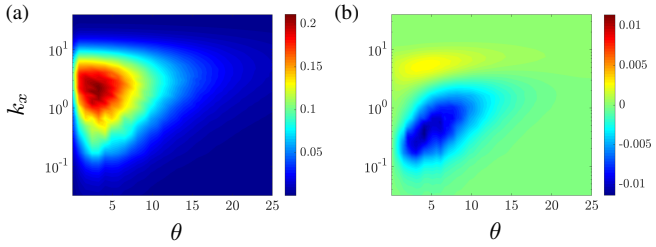

Fig. 5. (a) Premultiplied energy spectrum $k_x E_0(k_x, \theta)$ from numerical simulations of a turbulent channel flow with $Re_\tau = 186$ [33]; and (b) correction to the energy spectrum resulting from second-order statistics $X_c(k_x, \theta_n)$ for flow over triangular riblets with $\omega_z = 50$ ($l_g^+ = 9.9$).

dimensions, we parameterize Eqs. (12) using 48 streamwise Fourier wavenumbers ($0.03 < k_x < 40$) and $\theta_n = n\omega_z + \theta$ with $\omega_z = \{30, 35, 40, 45, 50, 60, 80, 100, 160\}$, respectively. To capture triangular riblets, we use Eq. (6) with 25 harmonics ($m = -12, \ldots, 12$).

We quantify the size of riblets using the obstruction area defined in inner units $l_g^+ := \sqrt{h^+ s^+/2}$, with h^+ and s^+ being the height and spacing in inner viscous units ($h^+ = Re_\tau h$ and $s^+ = Re_\tau s$). For triangular riblets of various size, Fig. 4(a) shows drag reduction ΔD (Eq. 9) normalized by its slope m_l at small l_g^+. It is clear that small-size riblets can indeed yield a decrease in turbulent drag. We observe good agreement in capturing the overall trend and the riblet size corresponding to maximum drag reduction from the experiments of [1] and the numerical simulations of [8], [10]. Figure 4(b) shows the turbulent kinetic energy suppression

$$\Delta E := \left(\bar{E} - E_0\right)/E_0$$

due to triangular riblets of various size. Here, $\bar{E}$ and E_0 denote the kinetic energy of velocity fluctuations in the presence and absence of riblets, respectively, which can be computed by integrating the energy spectrum $E(k_x, \theta)$ over all horizontal wavenumbers k_x and θ_n. Interestingly, we observe a very similar trend for ΔE as a function of l_g^+ to that of ΔD, which suggests that the kinetic energy of velocity fluctuations can be used as a surrogate for predicting the effect of surface corrugation on skin-friction drag.

Figure 5 compares the energy spectrum of turbulent channel flow with smooth walls and the change to the energy spectrum due to riblets. The energy spectra are premultiplied by the logarithmically scaled streamwise wavenumber so that the areas under the plots are equal to the total energy of fluctuations. Note that in the spanwise direction, which involves the parameterization $\theta_n = n\omega_z + \theta$, we have integrated the energy spectrum over all n. As shown in Fig. 5(a), the peak of the energy spectrum happen at $(k_x, \theta) = (2.2, 3.1)$. On the other hand, Fig. 5(b) shows that riblets with $\omega_z = 50$ reduce the energy at longer streamwise wavelengths (smaller k_x) and increase the energy at shorter ones; the largest energy amplification and suppression occur at $(k_x, \theta) = (5.5, 4.1)$ and $(k_x, \theta) = (0.4, 4.1)$, respectively. These figures provide evidence that the analysis of a spatially periodic system such as the one described in this paper cannot be limited to a single horizontal wavenumber pair associated with the peak of the energy spectrum or the dominant near-wall structures (cf. [23]). Similar conclusions were drawn in the analysis of channel flow subject to transverse wall oscillations [21].

V. Conclusion

We have developed a model-based framework for studying the effect of surface corrugation on skin-friction drag in turbulent channel flows. The influence of the corrugated surface is captured via a volume penalization technique. Our simulation-free approach is based on the utility of stochastically forced linearized equations in modeling the dynamics of velocity fluctuation and correcting turbulence models that capture the effect of background turbulence on the mean flow and skin-friction drag. For a turbulent channel flow with lower-wall spanwise-periodic triangular corrugation, we capture drag-reducing trends and optimal riblet sizes (producing maximum drag reduction) that have been previously reported in experimental and numerical studies. We also investigate the dependence of the turbulent kinetic energy of velocity fluctuations on the riblets' size and demonstrate very similar trends to what we observe for drag reduction. Our approach paves the way for an in-depth analysis of the underlying physical mechanisms that are responsible for drag reduction and energy suppression as well as the optimal design of riblet-mounted surfaces.

Appendix

A. Matrix operators A_θ and C_θ in Eqs. (12)

The generator A_θ has a bi-infinite structure of the form

$$A_\theta := \begin{bmatrix} \ddots & \vdots & \vdots & \vdots & \iddots \\ \cdots & A_{n-1,0} & A_{n-1,+1} & A_{n-1,+2} & \cdots \\ \cdots & A_{n,-1} & A_{n,0} & A_{n,+1} & \cdots \\ \cdots & A_{n+1,-2} & A_{n+1,-1} & A_{n+1,0} & \cdots \\ \iddots & \vdots & \vdots & \vdots & \ddots \end{bmatrix}$$

where the off-diagonal term $A_{n,m}$ denotes the influence of the $(n+m)$th harmonic $\boldsymbol{\psi}_{n+m}$ on the dynamics of the nth harmonic $\boldsymbol{\psi}_n$. Each $A_{n,m}$ contains four operators,

$$A_{n,m} = \begin{bmatrix} A_{n,m,1,1} & A_{n,m,1,2} \\ A_{n,m,2,1} & A_{n,m,2,2} \end{bmatrix}.$$

For $m = 0$, we have

$$A_{n,0,1,1} = \Delta_n^{-1}\left[(1+\nu_T)\Delta_n^2 + \nu_T''(\partial_y^2 + k_n^2) + \frac{2\nu_T'}{Re_\tau}\right] + \Gamma_{n,0,1,1},$$

$$A_{n,0,1,2} = \Gamma_{n,0,1,2},$$

$$A_{n,0,2,1} = \Gamma_{n,0,2,1},$$

$$A_{n,0,2,2} = \Delta_n^{-1}\left[(1+\nu_T)\Delta_n + \frac{\nu_T'}{Re_\tau}\right] + \Gamma_{n,0,2,2}$$

with $k_n^2 = k_x^2 + \theta_n^2$, and for $m \neq 0$, we have

$$A_{n,m,1,1} = \Gamma_{n,m,1,1}, \quad A_{n,m,1,2} = \Gamma_{n,m,1,2},$$
$$A_{n,m,2,1} = \Gamma_{n,m,2,1}, \quad A_{n,m,2,2} = \Gamma_{n,m,2,2}$$

where

$$\begin{aligned}
\Gamma_{n,m,1,1} &= \Delta_n^{-1}\Big[2\,\mathrm{i}m\,k_x\,\omega_z\frac{\theta_{n+m}}{k_{n+m}^2}\,(U_{-m}'\partial_y + U_{-m}\partial_{yy}) \\
&\quad + \mathrm{i}k_x\,(U_{-m}'' - U_{-m}\Delta_{n+m}) - a_{-m}\Delta_{n+m} \\
&\quad + \mathrm{i}k_x(m\,\omega_z)^2 U_{-m} - 2\,m\,k_x\omega_z\theta_{n+m}U_{-m} \\
&\quad + m\,\omega_z(m\omega_z - 2\,\theta_{n+m})a_{-m} - a_{-m}'\partial_y \\
&\quad + m\,\omega_z\frac{\theta_{n+m}}{k_{n+m}^2}\,(a_{-m}'\partial_y + a_{-m}\partial_{yy})\Big] \\
\Gamma_{n,m,1,2} &= \Delta_n^{-1}\left[2\,\frac{\mathrm{i}m\,k_x^2\,\omega_z}{k_{n+m}^2}\,(U_{-m}' + U_{-m}\partial_y)\right. \\
&\quad \left. + \frac{m\,k_x\,\omega_z}{k_{n+m}^2}\,(a_{-m}' + a_{-m}\partial_y)\right] \\
\Gamma_{n,m,2,1} &= \mathrm{i}m\,\omega_z\,(U_{-m}' - U_{-m}\partial_y) - \mathrm{i}\theta_{n+m}U_{-m}' \\
&\quad + \left[\mathrm{i}(m\,\omega_z)^2\frac{\theta_{n+m}}{k_{n+m}^2}\,U_{-m}' - \frac{m\,k_x\,\omega_z}{k_{n+m}^2}\,a_{-m}\right]\partial_y \\
\Gamma_{n,m,2,2} &= \Big[\Big(\frac{m\,\omega_z}{k_{n+m}}\Big)^2 - 1\Big]\mathrm{i}k_xU_{-m} + \Big[m\omega_z\frac{\theta_{n+m}}{k_{n+m}^2} - 1\Big]a_{-m}
\end{aligned}$$

Here, $\theta_{n+m} = (n+m)\omega_z + \theta$, $k_{n+m}^2 = k_x^2 + \theta_{n+m}^2$, and $\Delta_{n+m} = \partial_{yy} - k_{n+m}^2$. The operator C_θ is of the form

$$C_\theta = \mathrm{diag}\,\{\cdots, C_{n-1}, C_n, C_{n+1}, \cdots\}$$

where

$$C_n = \frac{1}{k_n^2}\begin{bmatrix} \mathrm{i}k_x\,\partial_y & -\mathrm{i}\,\theta_n \\ k_n^2 & 0 \\ \mathrm{i}\,\theta_n\,\partial_y & \mathrm{i}k_x \end{bmatrix}.$$

REFERENCES

[1] D. W. Bechert, M. Bruse, W. Hage, J. G. T. V. der Hoeven, and G. Hoppe, "Experiments on drag-reducing surfaces and their optimization with an adjustable geometry," *J. Fluid Mech.*, vol. 338, pp. 59–87, 1997.

[2] M. Gad-el Hak, *Flow control: passive, active, and reactive flow management*. New York: Cambridge University Press, 2000.

[3] E. Coustols and A. M. Savill, "Résumé of important results presented at the third turbulent drag reduction working party," *App. Sci. Res.*, vol. 46, no. 3, pp. 183–196, 1989.

[4] R. D. Joslin, "Aircraft laminar flow control," *Ann. Rev. Fluid Mech.*, vol. 30, pp. 1–29, 1998.

[5] M. Walsh, "Turbulent boundary layer drag reduction using riblets," in *20th aerospace sciences meeting*, 1982, p. 169.

[6] M. Walsh and A. Lindemann, "Optimization and application of riblets for turbulent drag reduction," in *22nd Aerospace Sciences Meeting*, 1984, p. 347.

[7] D. W. Bechert, M. Bruse, and W. Hage, "Experiments with three-dimensional riblets as an idealized model of shark skin," *Experiments in fluids*, vol. 28, no. 5, pp. 403–412, 2000.

[8] R. García-Mayoral and J. Jiménez, "Drag reduction by riblets," *Phil. Trans. R. Soc. A*, vol. 369, no. 1940, pp. 1412–1427, 2011.

[9] D. Goldstein and T.-C. Tuan, "Secondary flow induced by riblets," *J. Fluid Mech.*, vol. 363, pp. 115–151, 1998.

[10] R. García-Mayoral and J. Jiménez, "Hydrodynamic stability and breakdown of the viscous regime over riblets," *J. Fluid Mech.*, vol. 678, pp. 317–347, 2011.

[11] B. F. Farrell and P. J. Ioannou, "Stochastic forcing of the linearized Navier-Stokes equations," *Phys. Fluids A*, vol. 5, no. 11, pp. 2600–2609, 1993.

[12] B. Bamieh and M. Dahleh, "Energy amplification in channel flows with stochastic excitation," *Phys. Fluids*, vol. 13, no. 11, pp. 3258–3269, 2001.

[13] M. R. Jovanović and B. Bamieh, "Componentwise energy amplification in channel flows," *J. Fluid Mech.*, vol. 534, pp. 145–183, July 2005.

[14] W. Ran, A. Zare, M. J. P. Hack, and M. R. Jovanović, "Stochastic receptivity analysis of boundary layer flow," *Phys. Rev. Fluids*, vol. 4, no. 9, p. 093901 (28 pages), September 2019.

[15] Y. Hwang and C. Cossu, "Linear non-normal energy amplification of harmonic and stochastic forcing in the turbulent channel flow," *J. Fluid Mech.*, vol. 664, pp. 51–73, 2010.

[16] A. Zare, M. R. Jovanović, and T. T. Georgiou, "Colour of turbulence," *J. Fluid Mech.*, vol. 812, pp. 636–680, February 2017.

[17] A. Zare, T. T. Georgiou, and M. R. Jovanović, "Stochastic dynamical modeling of turbulent flows," *Annu. Rev. Control Robot. Auton. Syst.*, 2019, to appear; also arXiv:1811.09046.

[18] R. Moarref and M. R. Jovanović, "Controlling the onset of turbulence by streamwise traveling waves. Part 1: Receptivity analysis," *J. Fluid Mech.*, vol. 663, pp. 70–99, November 2010.

[19] B. K. Lieu, R. Moarref, and M. R. Jovanović, "Controlling the onset of turbulence by streamwise traveling waves. Part 2: Direct numerical simulations," *J. Fluid Mech.*, vol. 663, pp. 100–119, November 2010.

[20] M. R. Jovanović, "Turbulence suppression in channel flows by small amplitude transverse wall oscillations," *Phys. Fluids*, vol. 20, no. 1, p. 014101 (11 pages), January 2008.

[21] R. Moarref and M. R. Jovanović, "Model-based design of transverse wall oscillations for turbulent drag reduction," *J. Fluid Mech.*, vol. 707, pp. 205–240, September 2012.

[22] A. Kasliwal, S. Duncan, and A. Papachristodoulou, "Modelling channel flow over riblets: Calculating the energy amplification," in *Proceedings of 2012 UKACC International Conference on Control*, 2012, pp. 625–630.

[23] A. Chavarin and M. Luhar, "Resolvent analysis for turbulent channel flow with riblets," *AIAA Journal*, pp. 1–11, 2019.

[24] K. Khadra, P. Angot, S. Parneix, and J. Caltagirone, "Fictitious domain approach for numerical modelling of Navier-Stokes equations," *Int. J. Numer. Methods Fluids*, vol. 34, no. 8, pp. 651–684, 2000.

[25] W. D. McComb, *The Physics of Fluid Turbulence*. Oxford University Press, 1991.

[26] M. Luhar, "Low-order models for turbulent flows over complex walls," in *Tenth International Symposium on Turbulence and Shear Flow Phenomena (TSFP-10)*, 2017.

[27] W. V. R. Malkus, "Outline of a theory of turbulent shear flow," *J. Fluid Mech.*, vol. 1, no. 5, pp. 521–539, 1956.

[28] R. D. Cess, "A survey of the literature on heat transfer in turbulent tube flow," *Westinghouse Research, Rep. 8-0529-R24*, 1958.

[29] W. C. Reynolds and W. G. Tiederman, "Stability of turbulent channel flow with application to Malkus's theory," *J. Fluid Mech.*, vol. 27, no. 2, pp. 253–272, 1967.

[30] J. A. C. Weideman and S. C. Reddy, "A MATLAB differentiation matrix suite," *ACM Trans. Math. Software*, vol. 26, no. 4, pp. 465–519, December 2000.

[31] J. L. Aurentz and L. N. Trefethen, "Block operators and spectral discretizations," *SIAM Rev.*, vol. 59, no. 2, pp. 423–446, 2017.

[32] S. B. Pope, *Turbulent flows*. Cambridge University Press, 2000.

[33] J. C. Del Álamo and J. Jiménez, "Spectra of the very large anisotropic scales in turbulent channels," *Phys. Fluids*, vol. 15, no. 6, pp. 41–44, 2003.

[34] J. C. Del Álamo, J. Jiménez, P. Zandonade, and R. D. Moser, "Scaling of the energy spectra of turbulent channels," *J. Fluid Mech.*, vol. 500, no. 1, pp. 135–144, 2004.